LETTERS
https://doi.org/10.1038/s41556-021-00664-3
nature cell biology

Check for updates

Endothelial struts enable the generation of large lumenized blood vessels de novo

Bart Weijts[1,2]✉, Iftach Shaked[3,4], Mark Ginsberg[5], David Kleinfeld[3,4], Catherine Robin[2,6] and David Traver[1]✉

De novo blood vessel formation occurs through coalescence of endothelial cells (ECs) into a cord-like structure, followed by lumenization either through cell-[1–3] or cord-hollowing[4–7]. Vessels generated in this manner are restricted in diameter to one or two ECs, and these models fail to explain how vasculogenesis can form large-diameter vessels. Here, we describe a model for large vessel formation that does not require a cord-like structure or a hollowing step. In this model, ECs coalesce into a network of struts in the future lumen of the vessel, a process dependent upon bone morphogenetic protein signalling. The vessel wall forms around this network and consists initially of only a few patches of ECs. To withstand external forces and to maintain the shape of the vessel, strut formation traps erythrocytes into compartments to form a rigid structure. Struts gradually prune and ECs from struts migrate into and become part of the vessel wall. Experimental severing of struts resulted in vessel collapse, disturbed blood flow and remodelling defects, demonstrating that struts enable the patency of large vessels during their formation.

Cord-hollowing during vasculogenesis can either occur through fusion of intracellular lumens (formed through pinocytosis) of endothelial cells (ECs) connected in a head-to-tail orientation[1–3] or through the formation of an extracellular lumen between two ECs. This latter model depends on apical–basal polarization of ECs, which leads to the rearrangement of cell–cell junctions to the periphery of two adjacent ECs. Delivery of negatively charged glycoproteins to the apical side of the cells subsequently leads to the formation of a lumen between two ECs through electrostatic repulsion[4,5]. Alternatively, this extracellular lumen could also result from apical exocytosis of vacuoles[6]. As a result, the diameter of these vessels is restricted to either one (intracellular lumen) or two ECs (extracellular lumen). However, because vasculogenesis can result in the formation of large vessels, it raises the question of how these vessels acquire their large diameters. A good example of such a large-diameter vessel is the posterior cardinal vein (PCV), which forms along with the dorsal aorta (DA) the first blood vessels in the developing vertebrate embryo. In zebrafish, the caudal portion of the PCV, posterior to the yolk sac extension, is referred to as the caudal vein (CV) and is approximately five times larger than the DA and thus the largest blood vessel observed during development. Despite this large difference in diameter, the DA and PCV are formed and become functional over a nearly equivalent time-frame, suggesting that the lumen of the CV is probably not formed by one of the currently known mechanisms. To investigate how the CV is formed, we visualized its formation from 18 hours post fertilization (h.p.f.) onwards, the time point when ECs start to form the DA and CV at the midline of the embryo[8]. For visualization purposes, we focused either on the area of lumen formation (Fig. 1a, orange box) or vessel wall formation (Fig. 1a, green box). Around 18 h.p.f., the most medially positioned ECs started to coalescence into a network spanning the future lumen of the CV (Fig. 1b, orange boxes and Supplementary Video 1, left panel). Most branches of this network are composed of multiple ECs (Extended Data Fig. 1a). By time-lapse imaging, we found that this network gradually prunes and disappears from the lumen by 26–28 h.p.f. (Fig. 1b (orange boxes), 1c (blue area), Extended Data Fig. 1b and Supplementary Video 1, left panel). The wall of the CV is initially composed of only a few patches of ECs (18 h.p.f.), in stark contrast with the current models of vasculogenesis, in which the vascular cord already forms a 'leak-proof' vessel before lumenization (Fig. 1b, green boxes and Supplementary Video 1, right panel). Given that closure of the vessel wall coincided with pruning of the endothelial network, we hypothesized that ECs from the network are reused to form the CV wall. To test this hypothesis, we traced ECs within individual branches of the network by ultraviolet photoconversion of the DENDRA2 fluorescent protein from green to red. We found that the majority of the converted ECs (in 17 of 25 embryos) had integrated into the wall of the CV 20 h after conversion (Fig. 1d). In roughly 30% of the cases, we found that converted cells integrate into the arterial system, with ECs integrated into the floor of the DA or as single cells in the sub-aortic space between the DA and PCV, a typical appearance of haematopoietic stem and progenitor cells (Fig. 1e)[9,10]. Thus, the CV is formed around a temporary network of both arterial and venous ECs, which seems to maintain the patency of the CV. Hence, we termed these structures endothelial struts. Of note, we also found struts in the anterior part of the PCV, consisting only of 1–2 ECs, consistent with the smaller diameter relative to the posterior CV (Extended Data Fig. 1c). Furthermore, we did not find any evidence of EC proliferation or apoptosis during the formation or pruning of struts, suggesting that, through an intricate mechanism of ECs coalescing into struts, pruning and EC migration, large-diameter blood vessels can be formed without the need to expand the initial pool of ECs (Extended Data Fig. 1d).

Our photoconversion experiments suggested that struts in the CV contained arterial ECs (Fig. 1e). This finding is intriguing, because arterial and venous precursors arise from two distinct locations

[1]Section of Cell and Developmental Biology, Division of Biological Sciences, University of California–San Diego, La Jolla, CA, USA. [2]Hubrecht Institute, Royal Netherlands Academy of Arts and Sciences (KNAW) and University Medical Center Utrecht, Utrecht, Netherlands. [3]Department of Physics, University of California at San Diego, La Jolla, CA, USA. [4]Section of Neurobiology, University of California at San Diego, La Jolla, CA, USA. [5]Department of Medicine, University of California, San Diego, La Jolla, CA, USA. [6]Regenerative Medicine Center, University Medical Center Utrecht, Utrecht, Netherlands.
✉e-mail: b.weijts@hubrecht.eu; dtraver@ucsd.edu

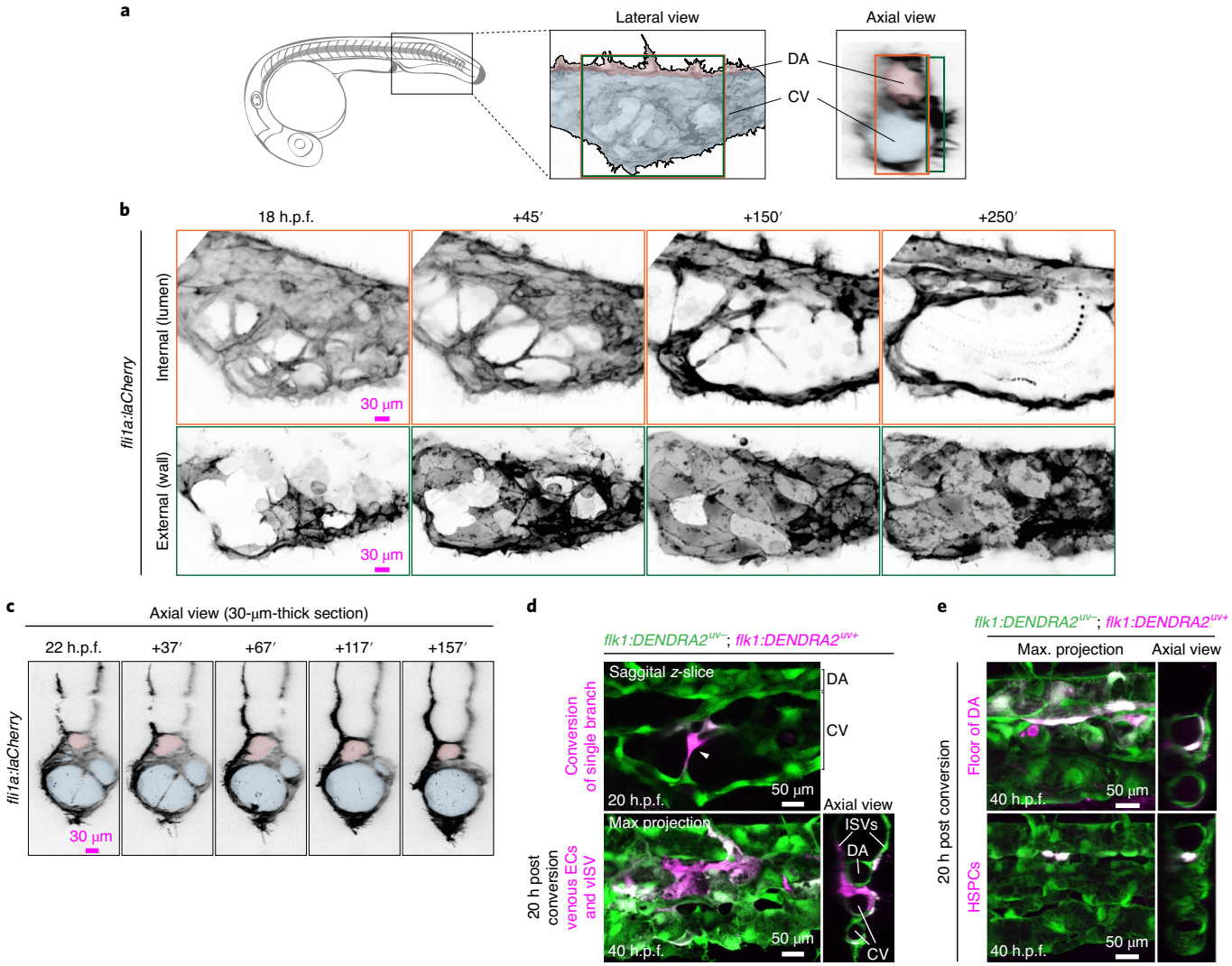

Fig. 1 | Formation of the caudal vein is facilitated through endothelial struts. a, Schematic of a 24 h.p.f. embryo. Orange (lumen) and green (vessel wall) boxes indicate visualized regions. The lumen of the DA and CV are pseudo-coloured in red and blue, respectively. The anterior is oriented to the left for all imaging data in this study unless stated otherwise. The images are representative of 30 analysed embryos from three independent experiments. **b**, Stills of Supplementary Video 1. In the orange panels, ECs are labelled with LifeActCherry (laCherry) under the control of the endothelial specific promoter *fli1a*. Formation and pruning of endothelial struts within the future lumen of the CV are shown. The green panels show the formation of the vessel wall of the CV. The stills are representative of five independent time-lapse experiments in which one embryo is imaged each. **c**, Axial view during the formation of the CV. Lumen of the DA and CV are pseudo-coloured in red and blue, respectively. The images are representative of 25 analysed embryos. **d**, Lineage tracing of ECs from struts by photoconversion of DENDRA2 (green to red). The images are representative of 30 analysed embryos from three independent experiments. In 68% of the embryos (17/25), the converted ECs were traced into the wall of the CV. The white arrowhead indicates the strut. ISVs, intersegmental vessels. **e**, In 24% of the cases, converted ECs were part of the floor of the DA (6/25) or the haematopoietic system (haematopoietic stem and progenitor cells (HSPCs)) (2/25). Scale bars are defined in the figure.

in the lateral plate mesoderm and were hypothesized to form the DA and PCV as independent entities[11]. Our images from the trunk at 20 h.p.f. showed two separate populations in the anterior part of the trunk that become increasingly intermingled, without a clear separation in the posterior part of the trunk (CV region; Fig. 2a). The arterial and venous ECs in the CV region formed a common precursor vessel that, over time, unmixed into the DA and CV in an anteroposterior direction (Fig. 2b and Supplementary Video 2). We visualized arterial and venous ECs by imaging embryos in which arterial ECs were fluorescently labelled by the arterial-restricted Notch ligand *delta-like 4* (*dll4*)[12] or by fluorescent reporting of Notch activity (*Tp1*)[13]. Consistent with results from our photoconversion experiments, we found that some ECs in struts located within the CV expressed *dll4* or were positive for Notch activity (*Tp1*) (Fig. 2c,d). Of note, we observed that the majority of arterial ECs that were juxtaposed to the hypochord, forming the roof of the DA, had a higher GFP signal (*dll4*) and showed increased Notch activity (*Tp1*) compared to arterial ECs positioned more ventrally (Fig. 2c,d). These findings suggest that arterial ECs positioned against the hypochord have a stronger arterial signature than the more ventrally positioned arterial ECs, which include those forming endothelial struts. From this, we reasoned that unmixing of arterial and venous ECs in the CV occurs through the gradual increase of arterial genes in the more ventrally positioned arterial ECs, including struts. To test this, we inhibited arterial differentiation by abrogating Notch signalling through administration of

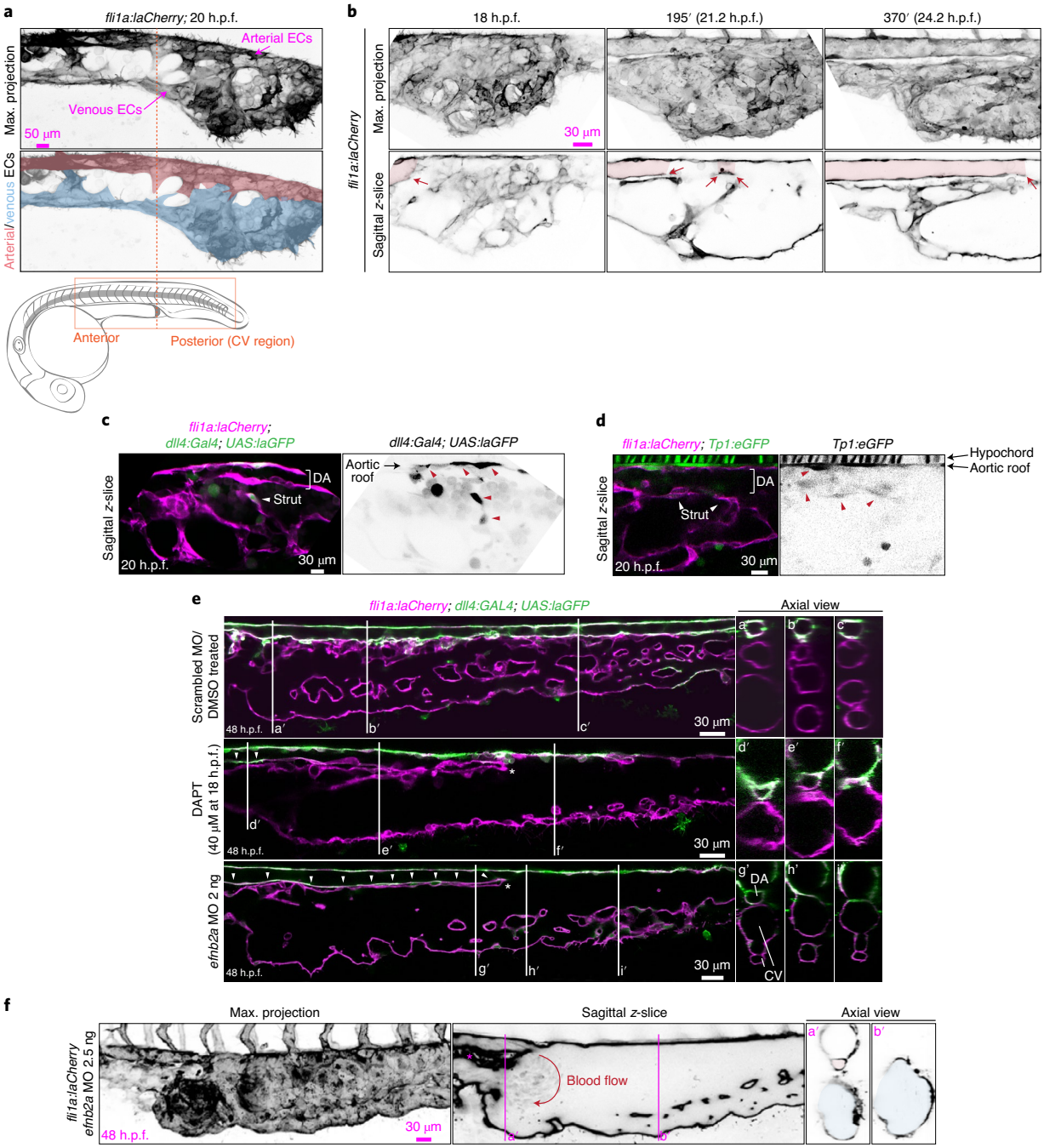

Fig. 2 | The caudal vein and dorsal aorta arise from a common precursor vessel through unmixing of arterial and venous ECs. a, Arterial and venous EC populations are indicated by anatomical position. The right panel shows pseudo-coloured populations. The images are representative of 20 analysed embryos from two independent experiments. **b**, Stills from Supplementary Video 2. The CV and DA are formed through segregation of arterial and venous ECs from a common precursor vessel. Red colour and arrows depict the formation of the DA lumen. The stills are representative of five independent time-lapse experiments in which one embryo is imaged each. **c**, Arterial ECs are marked by GFP (*dll4*; red arrowheads), all ECs are marked by laCherry (magenta) and the white arrowhead depicts the strut. The images are representative of 20 analysed embryos from two independent experiments. **d**, Notch signalling is reported by the expression of eGFP under the control of 12xCSL Notch-responsive elements (*Tp1*, red arrowheads), all ECs are marked by laCherry (magenta) and white arrowheads depict struts. The images are representative of 20 analysed embryos from two independent experiments. **e**, Chemical inhibition of the Notch signalling pathways by DAPT treatment or morpholino oligonucleotide (MO)-mediated knockdown of the downstream Notch target *ephrinb2a* in embryos in which arterial cells are marked by GFP (*dll4*) and all ECs by laCherry (magenta). As a control, a scrambled MO was injected at the same concentration as *efnb2a* MO or embryos were treated with the same concentration of DMSO in which the DAPT was dissolved. White arrowheads point at GFP (*dll4*) positive cells in the floor of the DA. Asterisks mark the disruption in arterial and venous unmixing. All images are representative of 20 analysed embryos from two independent experiments. **f**, A higher dose of *efnb2a* MO than in **e** results in a more dramatic unmixing phenotype. The magenta asterisk shows the disruption in arterial and venous unmixing and the red arrow shows the direction of blood flow. Note how some erythrocytes have faint laCherry expression, enabling visualization of the circulation. The images are representative of 30 analysed embryos from three independent experiments. Scale bars are defined in the figure.

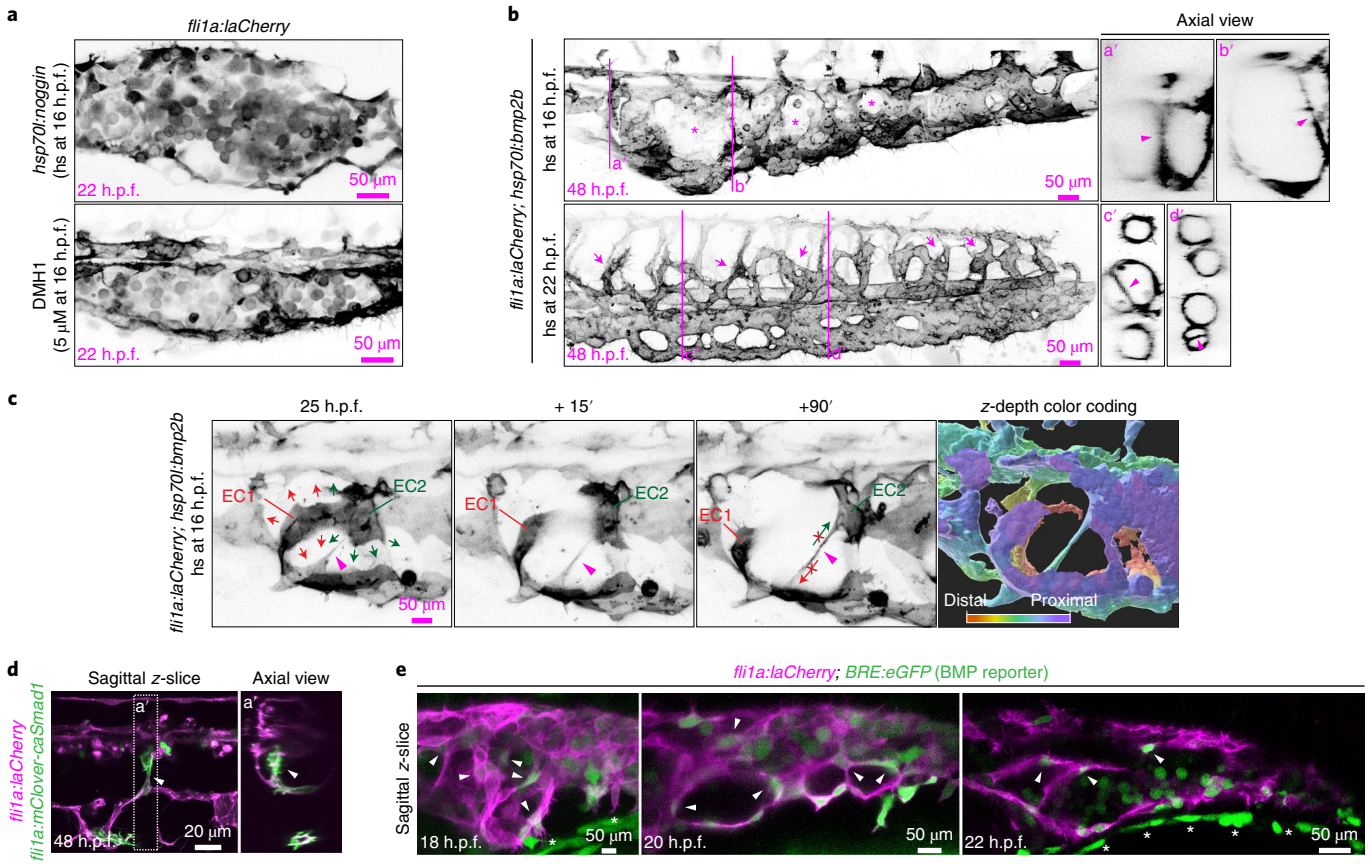

Fig. 3 | Bone morphogenetic protein signalling is required for strut formation. a, Inhibition of BMP signalling by heatshock (hs) inducible expression of *noggin* (heatshock at 16 h.p.f.) or administration of 50 µM DMH1 from 16 h.p.f. onwards. The images are representative of 20 analysed embryos from two independent experiments. **b**, Ectopic expression of *bmp2b* by heatshock at 16 h.p.f. (upper) or 22 h.p.f. (lower). Asterisks indicate a partially formed CV wall, arrowheads indicate struts and arrows indicate a previously described venous sprouting phenotype[19]. The images are representative of 30 analysed embryos from three independent experiments. **c**, Stills of Supplementary Video 3: ectopic expression of *bmp2b*, heatshock at 16 h.p.f., prevents struts from pruning and consequently closure of the vessel wall. Arrowheads indicate struts and red and green arrows the migration direction of two ECs. The rightmost panel shows surface rendering with *z*-depth colour coding. The stills are representative of two independent time-lapse experiments in which one embryo is imaged each. **d**, Constitutively active Smad1 fused to mClover (green) under the control of the EC specific promoter *fli1a* was injected for mosaic expression in *Tg*(*fli1a:laCherry*) embryos in which all ECs are marked by laCherry (magenta). Arrowheads indicate the mClover-caSmad positive strut. The images are representative of 30 analysed embryos from three independent experiments. **e**, Different developmental stages of embryos in which all ECs are marked by laCherry (magenta) and bmp activity is reported by eGFP. Arrowheads indicate GFP-positive struts. Note the GFP-positive erythrocytes within the CV region and the high expression of GFP by epithelial cells (asterisks). The images are representative of 20 analysed embryos from two independent experiments. Scale bars are defined in the figure.

the γ-secretase inhibitor DAPT[14]. In a complementary approach, we used a morpholino oligonucleotide (MO) to knock down the downstream Notch target *ephrinB2a* (*efnb2a*), which demarcates arterial and venous boundaries[15–17]. In both experiments, we found a dose-dependent inhibition of arterial–venous unmixing, resulting in a DA and PCV that remained fused (Fig. 2e,f and Extended Data Fig. 2a). The loss of Notch signalling in DAPT-treated embryos was illustrated by the marked reduction of *dll4* expression, which we did not observe in *efnb2a* morphants, a downstream Notch target gene (Fig. 2e, arrowheads). Importantly, inhibition of arterial specification did not affect strut formation or pruning (Extended Data Fig. 2b). Thus, a single precursor vessel is formed by arterial and venous ECs in the CV region, with struts of either EC type, which over time unmixes into the DA and CV through increasing expression of arterial genes like *efnb2a*.

Because bone morphogenetic protein (BMP) plays a pivotal role in the remodelling of the CV into the CV plexus, a process that starts after the CV becomes functional[18–20], we tested whether or not BMP signalling also plays a role in strut formation. To this end, we inhibited BMP signalling by expressing the BMP antagonist *noggin* via a *Tg*(*hsp70:noggin*) transgene[19] or treatment with the small molecule DMH1, a dorsomorphin analogue[21]. Alternatively, we ectopically activated the bmp pathway by expressing *bmp2b* via the *Tg*(*hsp70:bmp2b*) transgene[22]. *Noggin* and *bmp2b* expression were controlled by the heatshock inducible promoter (*hsp70*) and thereby allowed for manipulation of BMP signalling after the BMP-dependent specification of the dorsoventral mesoderm[23,24]. Genetic or chemical inhibition of BMP signalling from 16 h.p.f. onwards resulted in a failure of the ECs to coalesce into struts (Fig. 3a). Next, we ectopically expressed *bmp2b* from 16 h.p.f. onwards and found that a portion of the struts were still present at 48 h.p.f. (Fig. 3b, top), whereas in wild-type embryos all struts were cleared from the lumen by 26–28 h.p.f. (Fig. 1b,c). In addition, we found that the CV wall in these embryos was only partially formed, which may be explained by the inability of ECs in struts to migrate into the CV wall (Fig. 3b, asterisk, 3c and Supplementary Video 3). Ectopic expression of *bmp2b* between 18 and 22 h.p.f. disrupts cardiac morphogenesis[22] and, to circumvent this cardiac phenotype,

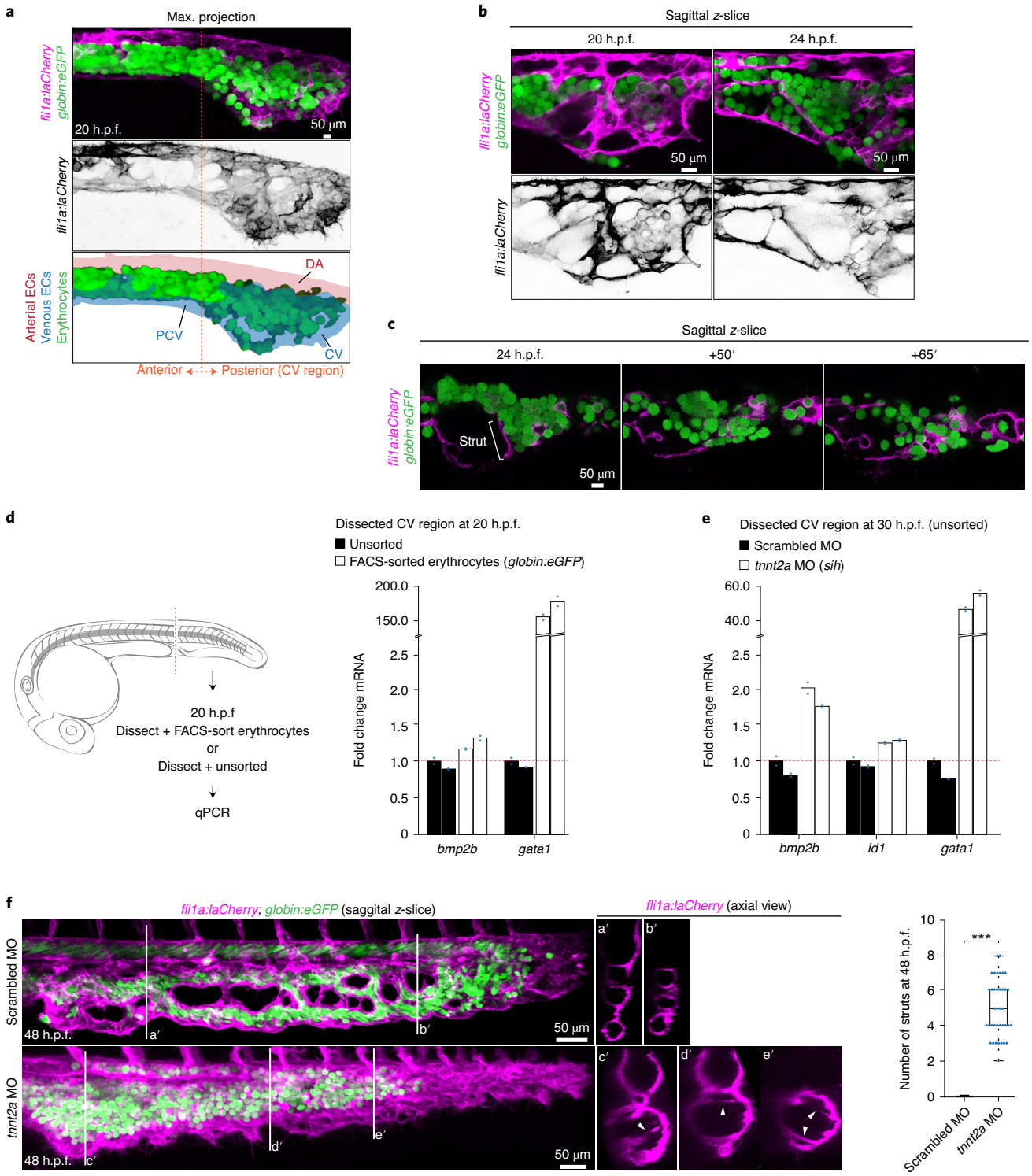

Fig. 4 | Struts compartmentalize the caudal vein and trap erythrocytes. a, Visualization of erythrocytes by eGFP (*globin*) and all ECs by laCherry (magenta) in the trunk during strut formation. The images are representative of 30 analysed embryos from three independent experiments. **b**, Strut formation compartmentalizes the CV, thereby trapping erythrocytes into compartments. The images are representative of 30 analysed embryos from three independent experiments. **c**, Stills of Supplementary Video 4: pruning of struts results in the release of erythrocytes into the circulation. The stills are representative of five independent time-lapse experiments in which one embryo is imaged each. **d**, qPCR on dissected CV regions and FACS-sorted erythrocytes (10 CVs were pooled per condition measured in two independent experiments). **e**, qPCR on dissected CV regions from embryos injected with a scrambled MO or *tnnt2a* MO to prevent the onset of circulation (10 CVs were pooled per condition measured in two independent experiments). **f**, Embryos injected with a scrambled MO or *tnnt2a* MO. Arrowheads indicate struts that failed to prune. The images are representative of 20 embryos analysed from two independent experiments. The boxplot on the right shows the quantification of the number of struts at 48 h.p.f. ($n = 15$ for scrambled MO and $n = 38$ for *tnnt2a* MO injected; data are from two independent repeats and presented as the median values with the first and third quartiles; the whiskers represent the minimum and maximum. Two-tailed Student's *t*-test. $^{***}P < 0.0001$). Scale bars are defined in the figure.

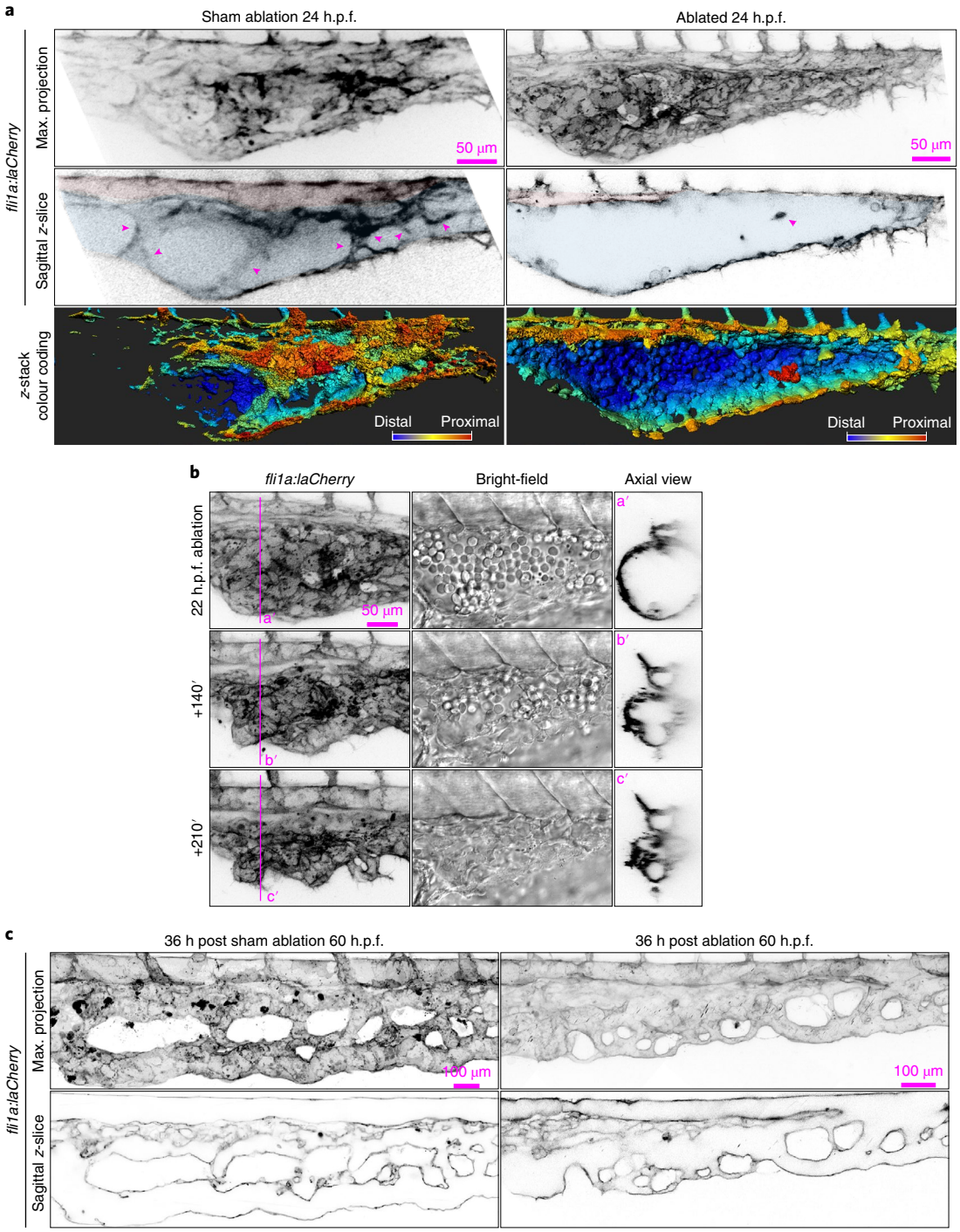

Fig. 5 | Endothelial struts provide structural support to the caudal vein. a, Laser ablation of endothelial struts. In sham-treated animals, the laser was fired ~25–50 µm from the strut in the empty space of the lumen, applying the same number of ablation pulses as in treated embryos. Ablation was carried out with 25 pulses of 0.2 µJ delivered at 5 kHz. Arrowheads indicate struts. Lower panels show surface rendering with *z*-depth colour coding, with the most distant cells in blue and cells at the forefront in red. The images are representative of 18 analysed embryos from three independent experiments. **b**, Stills of Supplementary Video 7: ablation of endothelial struts results in the collapse of the CV after initiation of circulation. The stills are representative of three independent time-lapse experiments in which one embryo is imaged each. **c**, Embryos 36 h after sham treatment or laser ablation of struts. The images are representative of 18 analysed embryos from three independent experiments. Scale bars are defined in the figure.

we heatshocked at around 22 h.p.f. Of note, at this time, the majority of the struts have already been pruned and therefore we could only target the few remaining struts (Fig. 1b,c). Similar to the experiments performed at 16 h.p.f., we also found struts that persisted at 48 h.p.f., while heart formation and circulation showed no obvious defects (Fig. 3b, lower). In addition, these embryos also displayed a previously described ectopic sprouting phenotype (Fig. 3b, arrows in bottom panel)[19]. Bmp2b regulates cellular responses through interaction with BMP receptors type I and II, resulting in the phosphorylation of Smads 1, 5 and 8 (R-Smads),

followed by heterodimerization of these phosphorylated R-Smads with co-Smad4 and ultimately the regulation of a myriad of downstream transcriptional targets, such as the angiogenic factor *id1*[25–27]. To further test whether strut formation was facilitated through this canonical BMP pathway, we generated a constitutively active zebrafish Smad1 (caSmad1), placed under the control of the endothelial specific promoter fli1a, and injected it at the single cell stage for mosaic expression[28–30]. Similar to the ectopic expression of *bmp2b*, caSmad1-mCLover positive struts failed to prune and were still present at 48 h.p.f., while injections of mClover alone did not prevent pruning of the struts (Fig. 3d and Extended Data Fig. 3a). By using a bmp reporter *Tg*(*bre:eGFP*), we found that besides expression in epidermal cells and erythrocytes, ECs in struts have active bmp signalling at different stages of CV formation (Fig. 3e)[31]. This is further supported by the presence of mRNA transcripts of both bmp2b receptors (*bmpr2a* and *bmpr2b*) and the downstream bmp target *id1*, indicative of active bmp signalling, in sorted ECs from the CV (Extended Data Fig. 3b). Thus, there is a temporal window in which bmp signalling is required for the formation of EC struts in the CV. Prolonging this window via ectopic activation of bmp signalling prevents struts from pruning.

Pruning of endothelial struts coincides with the onset of blood flow, an important factor in vascular remodelling and endothelial cell fate determination[32–34]. To study blood flow in relation to endothelial struts, we simultaneously visualized erythrocytes and ECs during strut formation. At the onset of strut formation, erythrocytes were partially positioned between arterial and venous ECs and a large portion of the erythrocytes were mixed with venous ECs, especially in the CV region (Fig. 4a). As a result of this mixing, strut formation in the CV region trapped these erythrocytes into compartments, with some tightly packed with erythrocytes (Fig. 4b). The DA is initially devoid of erythrocytes (Fig. 4a,b; 20 h.p.f.) and they only start to enter the DA when blood flow is initiated (Fig. 4b; 24 h.p.f.). Although initially trapped in these compartments, erythrocytes are gradually released into the circulation when struts start to prune, resulting in progressive loss of these compartments (Fig. 4c and Supplementary Video 4). Erythrocytes have been shown to be a source of secreted growth factors and, given that they are closely associated with the ECs prior to strut formation, we questioned whether erythrocytes may be a source of the *bmp2b* that contributes to strut formation[35]. To test this, we first used fluorescence-activated cell sorting (FACS) to sort erythrocytes at the time of CV formation and found *bmp2b* expression by quantitative polymerase chain reaction (qPCR; Fig. 4d and Extended Data Fig. 4a). Of note, *bmp2b* is also expressed by the ventral mesoderm surrounding the CV, which is included in the unsorted population that we used as a reference[19]. Next, we prevented erythrocytes from leaving the CV by inhibiting the onset of circulation by either blocking the expression of *cardiac troponin T2a* (*tnnt2a*) or through administration of the muscle relaxant ms-222 (tricaine methanesulfonate). From these embryos, we dissected the CV region and measured a twofold increase in *bmp2b* expression, further supporting that the erythrocytes are a substantial source of *bmp2b* (Fig. 4e). We found no difference in the number of struts just before the onset of circulation (26 h.p.f.); however, at 48 h.p.f. we still observed the same number of struts as at 26 h.p.f. in embryos without circulation (Fig. 4f and Extended Data Fig. 4b). Furthermore, in these embryos the CV wall was also not fully formed, which is in line with our earlier findings that ECs from struts are reused to form the CV wall (Extended Data Fig. 4c, asterisks). In summary, we demonstrate that the erythrocytes secrete the Bmp2b that is required for strut formation, become trapped in compartments formed by struts and gradually enter circulation when these compartments are progressively lost through pruning of struts.

To test the functionality of struts, we ablated 1–2 cells within a single strut by ultrashort pulses of near-infrared laser light, which was sufficient to sever the strut. This technique has been shown to generate negligible heat transfer and collateral damage to neighbouring tissues[36,37]. Because of the anatomical structure of the CV, we could only reliably sever endothelial struts after 22–24 h.p.f. (Fig. 5a and Supplementary Video 5). Although struts perpendicular to the sagittal plane were often difficult to detect and sever, we were able to ablate, on average, 95% of all struts within the CV (Fig. 5a, arrowhead in the middle right panel and Supplementary Video 6). As a control, we sham-treated embryos by positioning the laser 25–50 µm from struts, in the empty space of the lumen, applying the same number of ablation pulses as in treated embryos. Severing of nearly all endothelial struts initially did not lead to a dramatic change in the shape of the lumen. However, at the onset of circulation, the lumen of the CV collapsed due to a nearly instantaneous removal of the erythrocytes from the CV (Fig. 5b, Extended Data Fig. 5a and Supplementary Video 7). This collapsed CV is severely mispatterned during the remodelling of the CV into the CV plexus, although it allowed some blood flow (Fig. 5c). In animals in which circulation has just initiated, ablating a single strut often resulted in the release of erythrocytes into the circulation, demonstrating that these compartments trap erythrocytes (Supplementary Video 5, embryo 2).

In summary, we have shown that strut formation traps erythrocytes into compartments, with some tightly packed with erythrocytes, and thereby forms a rigid network that withstands external forces and maintains the shape of the vessel. Pruning of struts occurs gradually, ensuring that not all erythrocytes enter the circulation simultaneously, which would result in collapse of the vessel (Extended Data Fig. 5b).

Online content

Any methods, additional references, Nature Research reporting summaries, source data, extended data, supplementary information, acknowledgements, peer review information; details of author contributions and competing interests; and statements of data and code availability are available at https://doi.org/10.1038/s41556-021-00664-3.

Received: 27 June 2019; Accepted: 5 March 2021;
Published online: 9 April 2021

References

1. Folkman, J. & Haudenschild, C. Angiogenesis in vitro. *Nature* **288**, 551–556 (1980).
2. Kamei, M. et al. Endothelial tubes assemble from intracellular vacuoles in vivo. *Nature* **442**, 453–456 (2006).
3. Davis, G. E. & Bayless, K. J. An integrin and Rho GTPase-dependent pinocytic vacuole mechanism controls capillary lumen formation in collagen and fibrin matrices. *Microcirculation* **10**, 27–44 (2003).
4. Strilić, B. et al. Electrostatic cell-surface repulsion initiates lumen formation in developing blood vessels. *Curr. Biol.* **20**, 2003–2009 (2010).
5. Ferrari, A., Veligodskiy, A., Berge, U., Lucas, M. S. & Kroschewski, R. ROCK-mediated contractility, tight junctions and channels contribute to the conversion of a preapical patch into apical surface during isochoric lumen initiation. *J. Cell Sci.* **121**, 3649–3663 (2008).
6. Blum, Y. et al. Complex cell rearrangements during intersegmental vessel sprouting and vessel fusion in the zebrafish embryo. *Dev. Biol.* **316**, 312–322 (2008).
7. Gebala, V., Collins, R., Geudens, I., Phng, L.-K. & Gerhardt, H. Blood flow drives lumen formation by inverse membrane blebbing during angiogenesis in vivo. *Nat. Cell Biol.* **18**, 443–450 (2016).
8. Hogan, B. M. & Schulte-Merker, S. How to plumb a pisces: understanding vascular development and disease using zebrafish embryos. *Dev. Cell* **42**, 567–583 (2017).
9. Bertrand, J. Y. et al. Haematopoietic stem cells derive directly from aortic endothelium during development. *Nature* **464**, 108–111 (2010).
10. Kissa, K. & Herbomel, P. Blood stem cells emerge from aortic endothelium by a novel type of cell transition. *Nature* **464**, 112–115 (2010).
11. Kohli, V., Schumacher, J. A., Desai, S. P., Rehn, K. & Sumanas, S. Arterial and venous progenitors of the major axial vessels originate at distinct locations. *Dev. Cell* **25**, 196–206 (2013).

12. Hermkens, D. M. A. et al. Sox7 controls arterial specification in conjunction with *hey2* and *efnb2* function. *Development* **142**, 1695–1704 (2015).
13. Parsons, M. J. et al. Notch-responsive cells initiate the secondary transition in larval zebrafish pancreas. *Mech. Dev.* **126**, 898–912 (2009).
14. Lawson, N. D. et al. Notch signaling is required for arterial-venous differentiation during embryonic vascular development. *Development* **128**, 3675–3683 (2001).
15. Adams, R. H. et al. Roles of ephrinB ligands and EphB receptors in cardiovascular development: demarcation of arterial/venous domains, vascular morphogenesis and sprouting angiogenesis. *Genes Dev.* **13**, 295–306 (1999).
16. Wang, H. U., Chen, Z. F. & Anderson, D. J. Molecular distinction and angiogenic interaction between embryonic arteries and veins revealed by ephrin-B2 and its receptor Eph-B4. *Cell* **93**, 741–753 (1998).
17. Herbert, S. P. et al. Arterial–venous segregation by selective cell sprouting: an alternative mode of blood vessel formation. *Science* **326**, 294–298 (2009).
18. Wakayama, Y., Fukuhara, S., Ando, K., Matsuda, M. & Mochizuki, N. Cdc42 mediates Bmp-induced sprouting angiogenesis through Fmnl3-driven assembly of endothelial filopodia in zebrafish. *Dev. Cell* **32**, 109–122 (2015).
19. Wiley, D. M. et al. Distinct signalling pathways regulate sprouting angiogenesis from the dorsal aorta and the axial vein. *Nat. Cell Biol.* **13**, 686–692 (2011).
20. Neal, A. et al. Venous identity requires BMP signalling through ALK3. *Nat. Commun.* **10**, 453 (2019).
21. Hao, J. et al. In vivo structure–activity relationship study of dorsomorphin analogues identifies selective VEGF and BMP inhibitors. *ACS Chem. Biol.* **5**, 245–253 (2010).
22. Chocron, S., Verhoeven, M. C., Rentzsch, F., Hammerschmidt, M. & Bakkers, J. Zebrafish Bmp4 regulates left-right asymmetry at two distinct developmental time points. *Dev. Biol.* **305**, 577–588 (2007).
23. Mullins, M. C. et al. Genes establishing dorsoventral pattern formation in the zebrafish embryo: the ventral specifying genes. *Development* **123**, 81–93 (1996).
24. Kishimoto, Y., Lee, K. H., Zon, L., Hammerschmidt, M. & Schulte-Merker, S. The molecular nature of zebrafish swirl: BMP2 function is essential during early dorsoventral patterning. *Development* **124**, 4457–4466 (1997).
25. Monteiro, R. et al. Two novel type II receptors mediate BMP signalling and are required to establish left–right asymmetry in zebrafish. *Dev. Biol.* **315**, 55–71 (2008).
26. Liu, F. et al. A human Mad protein acting as a BMP-regulated transcriptional activator. *Nature* **381**, 620–623 (1996).
27. Lyden, D. et al. Id1 and Id3 are required for neurogenesis, angiogenesis and vascularization of tumour xenografts. *Nature* **401**, 670–677 (1999).
28. Chen, X., Zaro, J. L. & Shen, W.-C. Fusion protein linkers: property, design and functionality. *Adv. Drug Deliv. Rev.* **65**, 1357–1369 (2013).
29. Kokabu, S., Katagiri, T., Yoda, T. & Rosen, V. Role of Smad phosphatases in BMP-Smad signaling axis-induced osteoblast differentiation. *J. Oral Biosci.* **54**, 73–78 (2012).
30. Lawson, N. D. & Weinstein, B. M. In vivo imaging of embryonic vascular development using transgenic zebrafish. *Dev. Biol.* **248**, 307–318 (2002).
31. Alexander, C. et al. Combinatorial roles for BMPs and endothelin 1 in patterning the dorsal–ventral axis of the craniofacial skeleton. *Development* **138**, 5135–5146 (2011).
32. Chen, Q. et al. Haemodynamics-driven developmental pruning of brain vasculature in zebrafish. *PLoS Biol.* **10**, e1001374 (2012).
33. Weijts, B. et al. Blood flow-induced Notch activation and endothelial migration enable vascular remodeling in zebrafish embryos. *Nat. Commun.* **9**, 5314 (2018).
34. Le Noble, F. et al. Flow regulates arterial–venous differentiation in the chick embryo yolk sac. *Development* **131**, 361–375 (2004).
35. Helker, C. S. M. et al. The zebrafish common cardinal veins develop by a novel mechanism: lumen ensheathment. *Development* **140**, 2776–2786 (2013).
36. Nishimura, N. et al. Targeted insult to subsurface cortical blood vessels using ultrashort laser pulses: three models of stroke. *Nat. Methods* **3**, 99–108 (2006).
37. Tsai, P. S. et al. Plasma-mediated ablation: an optical tool for submicrometer surgery on neuronal and vascular systems. *Curr. Opin. Biotechnol.* **20**, 90–99 (2009).

Methods

Zebrafish husbandry. Zebrafish (*Danio rerio*) were maintained and propagated according to the guidelines of the UCSD Institutional Animal Care and Use Committee and Hubrecht Institute Ethical Review Board. All animal experiments were approved by the Animal Experimentation Committee (DEC) of the Royal Netherlands Academy of Arts and Sciences. Embryos and adult fish were raised in a circulating aquarium system (Aquaneering) at 28 °C. The following zebrafish lines have been described previously: *Tg(fli1a:lifeactCherry)*^{ncv7Tg} (ref. [18]), referred to as fli1a:laCherry; *Tg(fli1a:eGFP)*^{y1} (ref. [30]); *Tg(hbbe1.1:EGFP)*^{zf446} (ref. [38]), referred to as *Tg(globin:eGFP)*; *Tg(flk:DENDRA2)* (ref. [39]); *Tg(dll4:Gal4FF)*^{hu10049Tg} (ref. [12]); *Tg(UAS:lifeactGFP)*^{mu271} (ref. [35]), referred to as UAS:laGFP; *Tg(EPV.Tp1-Mmu.Hbb:GFP-utrn)* (ref. [13]) referred to as *Tg(Tp1:GFP)*; *Tg(hsp70:bmp2b)*^{fr13} (ref. [22]); *Tg(kdrl:nlsGFP)*^{ubs1} (ref. [6]). Details on the strains and ages are noted for each experiment. Gender was not selected in any of the studies conducted.

Morpholino and plasmid injections, heatshock and chemical treatment. Embryos were injected at the one-cell stage with MOs (GeneTools) or 50 ng of plasmid with 100 ng of *tol2* mRNA: Ephrinb2a (efnb2a) translation blocking MO (5′-CGGTCAAATTCCGTTTCGCGGGA-3′)[40]; silent heart morpholino *tnnt2a* (5′-CATGTTTGCTCTGATCTGACACGCA-3′)[41]. Scrambled MO was injected at similar concentrations as the targeted MO (5′-CCTCTTACCTCAGTTACAATTTATA-3′). Capped tol2 mRNA was synthesized from linearized pCS2+ constructs using the mMessage mMachine SP6 kit (Ambion, AM1340). Injected and un-injected control embryos were heatshocked at 38 °C for 30 min. Embryos were treated with 50 µM DMH1 (#16679, Cayman Chemical), 40 µM DAPT (#13197, Cayman Chemical) dissolved in DMSO (1,000× stock solution) and control embryos were treated with DMSO alone. Blood flow was inhibited by treating the embryos with 0.48 mg ml^{-1} (3×) ethyl 3-aminobenzoate methanesulfonate (MS222; Sigma E10521). Live embryos were soaked in 10 µg ml^{-1} (Thermo Fisher A1301) dissolved in E3 medium for 30 min and extensively washed with E3 medium afterwards and subsequently imaged.

Microscopy and laser ablation. Live microscopy was carried out using environmentally controlled microscopy systems based on a Leica TCS SP5 or SP8 confocal microscope or a Zeiss LSM 880 with an Airyscan system. For all imaging, embryos were placed into a modified Four-Well WillCo dish[42] submerged in E3 medium containing 0.168 mg ml^{-1} = 0.0168% = ~0.02% ethyl 3-aminobenzoate methanesulfonate (MS222; Sigma E10521) at a temperature of 28.5 °C. Imaging was subsequently done with either ×20/0.75, ×40/1.4 or ×63/1.46 objectives.

For laser ablation experiments, embryos were embedded in 1% low-melting-point agarose (Invitrogen) in a WillCo dish with a 40-mm #1.5 cover glass bottom and placed under a two-photon laser scanning microscope of local design that included an amplified beam[43]. Laser ablation of endothelial struts was achieved by using targeted ultra-fast laser pulses that were generated with a multi-pass Ti:Al_2O_3 amplifier of local construction that followed a previously published design[36] and operated at a pulse rate of 5 kHz. The ablation beam and imaging beam were combined before the microscope objective with a polarizing beamsplitter[36]. We focused the two beams in the same focal plane and centred the ablation beam in the area that was raster-scanned by the imaging beam so that ablation occurred at the centre of the two-photon laser scanning microscopy (TPLSM) imaging field. The energy per pulse of the ablation beam was tuned with neutral density filters and the number of pulses was controlled by a mechanical shutter (Uniblitz LS3Z2 shutter and VMM-D1 driver; Vincent). The energy and number of pulses were modified based on damage assessed from the real-time TPLSM images. Ablation was carried out with 25 pulses of 0.2 µJ delivered at 5 kHz

Cloning. The coding sequence of zebrafish Smad1 (ENSDARG00000027199) was cloned into the pCS2+ vector by the Gibson cloning method (NEB HiFi DNA assembly mix, E2621S). To substitute serine 470 and 472 into aspartic acid (SVS to DVD), zfSmad1 was subcloned with reversed primers containing the required nucleotide changes (see Supplementary Table 1 for the primer sequences) and fused to mClover3 (N-terminally) spaced with the flexible linker GSAGSAAGSGEF in front of the fli1a endothelial specific promoter, referred to as *Tg(fli1a:mClover-caSmad1)*. The coding sequence of Ephrinb2a (ENSDARG00000020164) was cloned into the pCS2+ vector and mRNA was transcribed with the Sp6 message machine kit (Promega).

Cell preparation and flow cytometry. Embryos were collected and anaesthetized in E3 medium containing 0.01% tricaine, then the CV region or trunk region was dissected and placed in ice-cold PBS. After centrifugation, the pellet was washed with ice-cold PBS and resuspended in TrypLE (Thermo Fisher, 12563011) for 45 min at 32 °C with vigorous shaking. Cells were then washed with FACS buffer (PBS + 2% FBS + 2 mM EDTA), dissolved in FACS buffer + DAPI (Thermo Fisher, 0.5 µg ml^{-1} final concentration) and subsequently filtered through 40-µm nylon mesh. Cells were sorted on a FACS Aria II system (BD Biosciences) and collected in FACS buffer for gene expression analysis. Forward scatter (FSC) and side scatter (SSC) were cut at 50k and live cells were DAPI negative ($<5\times10^2$). The gating strategies for erythrocytes (GFP) and endothelial cells (mCherry) are shown in Extended Data Figs. 3b and 4a.

Quantitative PCR and PCR with reverse transcription. RNA was extracted from dissected tissue (CV region) or sorted cells using Trizol (Thermo Fisher), according to the manufacturer's instructions. cDNA was generated using GoScript (Promega) using random hexamer primers. qPCR assays were performed on a Bio-Rad CFX96 real-time system according to the manufacturer's instructions (Bio-Rad) with Fast SYBR Green (Bio-Rad). The expressions of ef1a, 18s, tbp and bactin were used to normalize the amount of the investigated transcripts. The primers used are listed in Supplementary Table 1.

Imaging. Images captured in Aryscan mode (Zeiss LSM 880 with Zeiss ZEN blue version 3.0) were first processed in Zeiss ZEN blue (Aryscan processing) and subsequent analysed using Fiji (version 1.52P) or Imaris (version 9.1). Sub-stacks were subtracted to specifically visualize the blood vessel wall or lumen, or *z*-stacks were flattened by the maximum intensity projection method used as stated in the figure captions. In some cases, *XY* drifts were corrected using the MultiStackReg plugin (Fiji; B. Busse, NICHD, version (1.15)) and correction of fluorescence bleaching by histogram matching (Fiji). Tiled images were stitched with either ZEN blue or Imaris sticher (version 9.1). Contrast in all images was adjusted and look-up tables (LUT) adjusted (red to magenta or red/green to black and white) in Fiji or Imaris for visualization purposes. Surface renderings were performed in Imaris. Figures, videos and animations were created with Adobe Illustrator, Photoshop, After Effects and Premier (version CS5).

Reagents. A list of reagents and catalogue numbers is provided in Supplementary Table 2.

Statistical analysis and experimental set-up. For each in vivo experiment, animals from the same clutch were divided into different treatment groups without any bias. The whole clutch was excluded if more than 10% of control embryos displayed obvious developmental defects. If necessary, statistical analysis was performed using SPSS version 20 (IBM). The Mann–Whitney U test was used for statistical analysis of two groups with unequal variances. The unpaired *t*-test was used for two groups with equal variances. The Kruskal–Wallis test was used for statistical analysis of multiple groups with equal variances, and one-way analysis of variance for multiple groups with unequal variances. Dunn's post-hoc test was used for pairwise multiple comparisons. All experiments are a representation of at least two independent repeats.

Reporting Summary. Further information on research design is available in the Nature Research Reporting Summary linked to this Article.

Data availability

Source data are provided with this paper. All other data supporting the findings of this study are available from the corresponding author upon reasonable request.

References

38. Ganis, J. J. et al. Zebrafish globin switching occurs in two developmental stages and is controlled by the LCR. *Dev. Biol.* **366**, 185–194 (2012).
39. Tian, Y. et al. The first wave of T lymphopoiesis in zebrafish arises from aorta endothelium independent of hematopoietic stem cells. *J. Exp. Med.* **214**, 3347–3360 (2017).
40. Cooke, J. E., Kemp, H. A. & Moens, C. B. EphA4 is required for cell adhesion and rhombomere-boundary formation in the zebrafish. *Curr. Biol.* **15**, 536–542 (2005).
41. Sehnert, A. J. et al. Cardiac troponin T is essential in sarcomere assembly and cardiac contractility. *Nat. Genet.* **31**, 106–110 (2002).
42. Weijts, B., Tkachenko, E., Traver, D. & Groisman, A. A four-well dish for high-resolution longitudinal imaging of the tail and posterior trunk of larval zebrafish. *Zebrafish* **14**, 489–491 (2017).
43. Tsai, P. S. & Kleinfeld, D. in *In Vivo Optical Imaging of Brain Function* (ed. Frostig, R. D.) (CRC Press/Taylor & Francis) Chapter 3, 56–116 (2009).

Acknowledgements

We thank the Animal Facility for zebrafish care (UCSD and Hubrecht Institute). We thank D. Yelon (University of California, San Diego) for the silent heart morpholino, S.-W. Jin (Yale Cardiovascular Research Center) for generously providing us with the hsp70l:noggin plasmid, J. Bakkers (Hubrecht Institute) for the hsp70:bmp2b line, J. den Hertog for the bre:egfp line and P. Tsai for use of the Q-bio laboratory confocal system. We thank J. Santini, N. Gohad (Zeiss) and K. Fertig (Leica) for microscopy technical assistance, the UCSD School of Medicine Microscopy Core, the Princess Máxima Imaging Center and the Hubrecht Institute Optical Imaging Center. This work was supported by the San Diego School of Medicine Microscopy Core (P30 NS047101). We thank R. van der Linden (Hubrecht Institute) for help with cell sorting. Part of this work was supported by a European Research Council grant (ERC project no. 220-H75001EU/HSCOrigin-309361; C.R.), a TOP subsidy from NWO/ZonMw (912.15.017; C.R.), NIH/NINDS R01NS108472 (I.S. and D.K.), NIH/NINDS R35NS097265 (I.S. and D.K.) and NIH R01DK074482 (D.T.).

Author contributions

B.W. designed, performed, analysed experiments and wrote the manuscript. Laser ablation experiments were performed by B.W. and I.S. under the supervision of D.K. M.G. interpreted data and designed experiments. Part of the project was supervised by C.R. D.T. supervised the project and wrote the manuscript. All authors discussed the results and commented on the manuscript at all stages.

Competing interests

The authors declare no competing interests.

Additional information

Extended data is available for this paper at https://doi.org/10.1038/s41556-021-00664-3.

Supplementary information The online version contains supplementary material available at https://doi.org/10.1038/s41556-021-00664-3.

Correspondence and requests for materials should be addressed to B.W. or D.T.

Peer review information *Nature Cell Biology* thanks M. Luisa Iruela-Arispe and the other, anonymous, reviewers for their contribution to the peer review of this work. Peer reviewer reports are available.

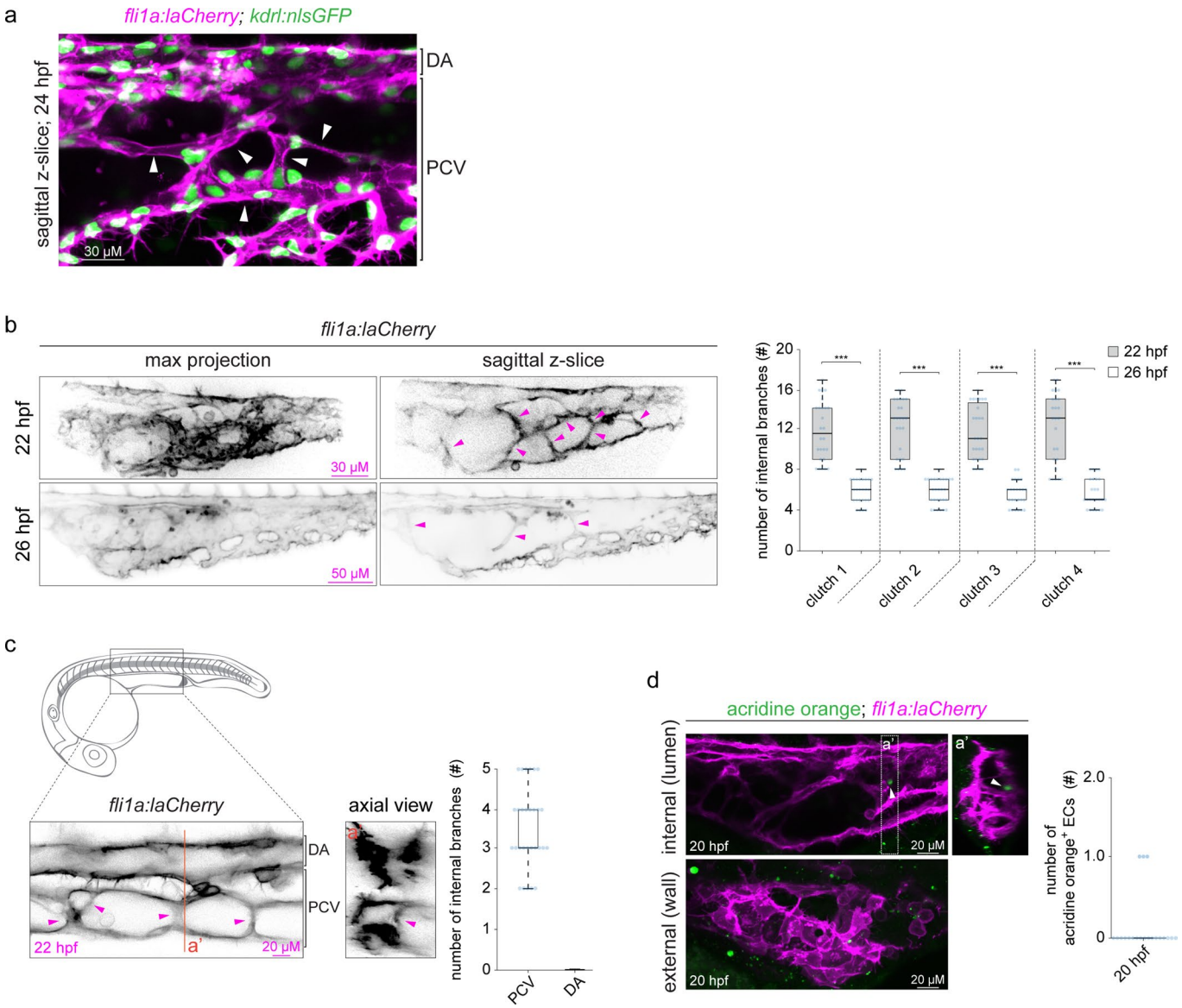

Extended Data Fig. 1 | Characterization of endothelial struts. a, All ECs are marked by both laCherry (magenta; cytoskeleton) and eGFP (green; nuclei). Struts are depicted by arrowheads. Images are representative of 20 embryos analysed from two independent experiments. **b**, Quantification of the number of endothelial struts at 22 hpf and 26 hpf by confocal microscopy and represented as the median values with the first and third quartiles; the whiskers represent the minimum and maximum (4 different clutches per time point (n = 26; n = 25; n = 27; n = 25 for 22 hpf and n = 25; n = 28; n = 25; n = 25 for 26 hpf. Two-tailed Student's *t*-test. ***$P < 0.0001$ for all 4 tests). Arrowheads depict endothelial struts. Images are representative of indicated groups from four independent experiments. **c**, Strut formation in the anterior part of the PCV at 22hpf by confocal microscopy and represented as the median values with the first and third quartiles; the whiskers represent the minimum and maximum (n = 30 embryos from three independent experiments). Arrowheads depict endothelial struts. **d**, Quantification of the number of acridine orange positive ECs in the CV region at 20 hpf and representative confocal images. White arrowhead depicts a positive EC (n = 20 embryos from two independent experiments). Scale bars are defined in the figure.

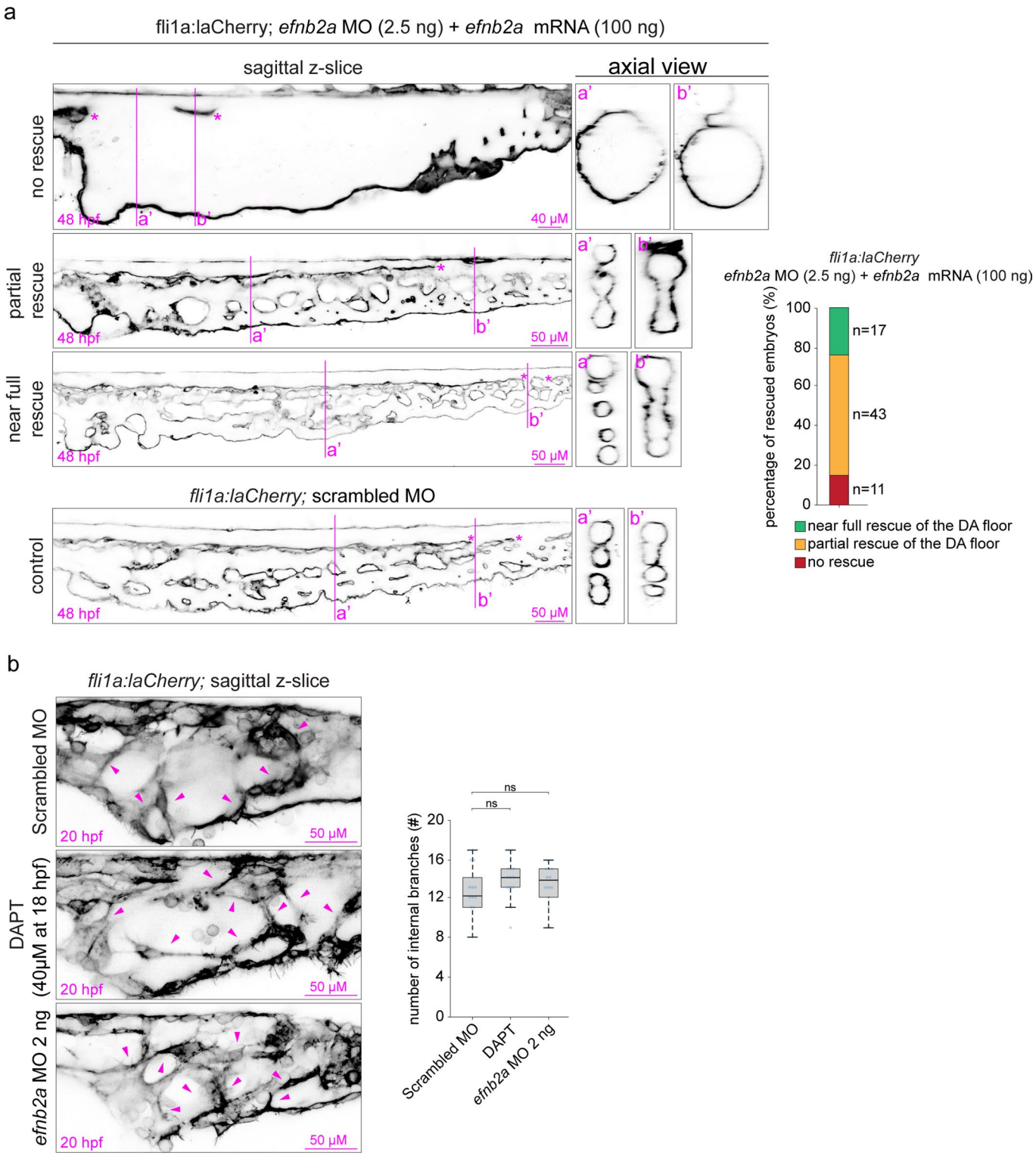

Extended Data Fig. 2 | Unmixing of arterial and venous endothelial cells. a, Rescue of ephrinb2a morphants with *efnb2a* mRNA. Embryos were grouped by the level of rescue (near full, partial or no rescue) of the floor of the DA, indicated by the asterisks. (n = 71 embryos analysed in one experiment, n numbers per group indicated in graph). Images are representative of 5 embryos analysed by confocal microscopy per group. **b**, Representative images and quantification of the number of struts in embryos treated with the Notch inhibitor DAPT or injected with an *ephnb2a* MO. As a control, embryos were injected with a scrambled MO. (n = 14 embryos per condition). Data presented as the median values with the first and third quartiles; the whiskers represent the minimum and maximum. Images are representative of 5 embryos analysed by confocal microscopy per condition. Scale bars are defined in the figure.

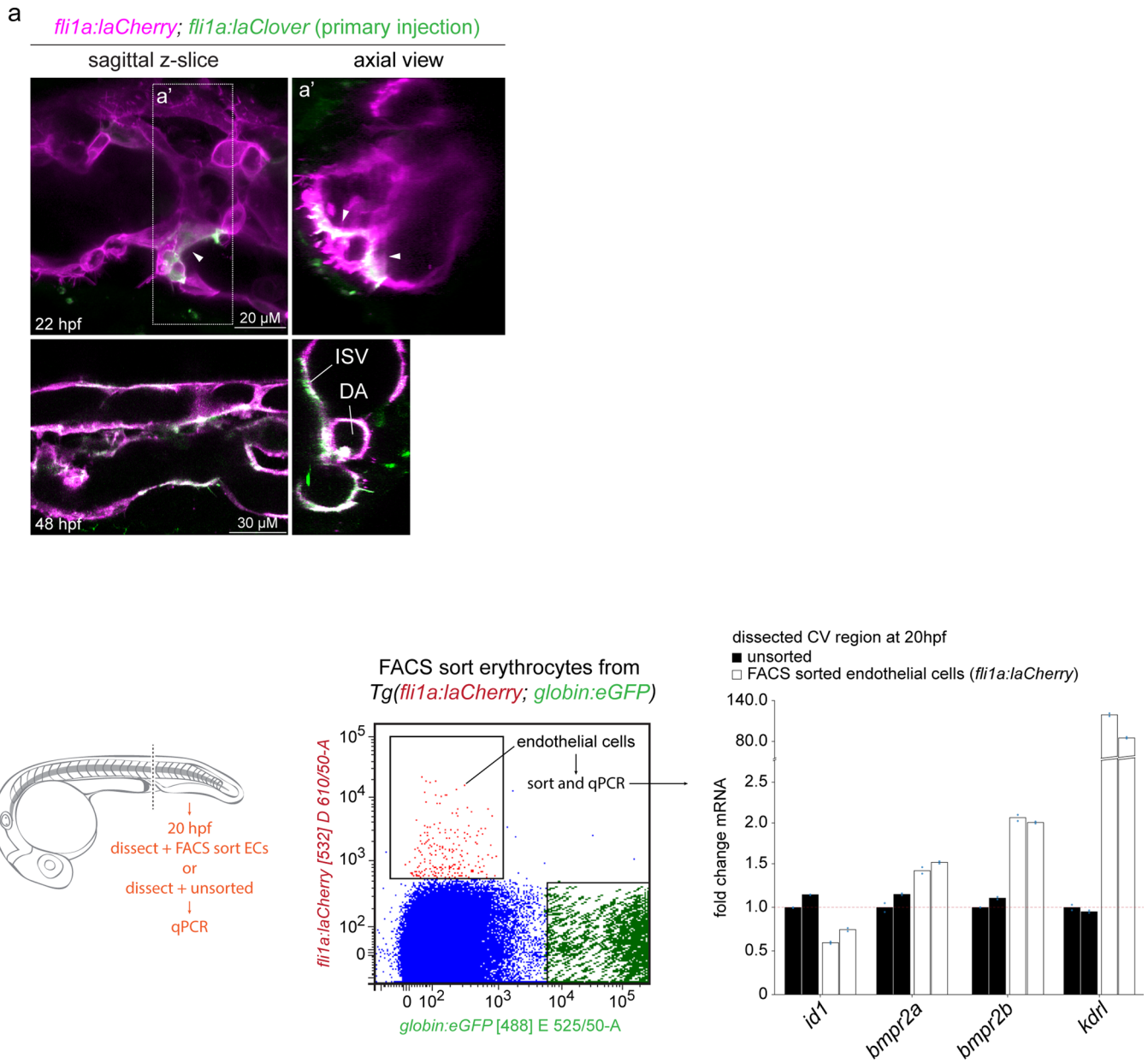

Extended Data Fig. 3 | BMP signalling is required for strut formation. a, Mosaic expression of laClover under the control of the EC specific promoter *fli1a*. Arrowhead indicates mClover positive strut at 22 hpf (upper panel). Lower panel shows an image of the same region at 48 hpf. Images are representative of 9 embryos analysed from three independent experiments. **b**, Gating strategy used to FACS sort ECs from dissected CV regions followed by qPCR (10 CVs were pooled per condition measured in two independent experiments). Of note, the bmp pathway is active in multiple tissues at this time, including erythrocytes and strong activity in epithelial cells (Fig. 3e asterisks), these cells are included in the unsorted CV (black bars). Scale bars are defined in the figure.

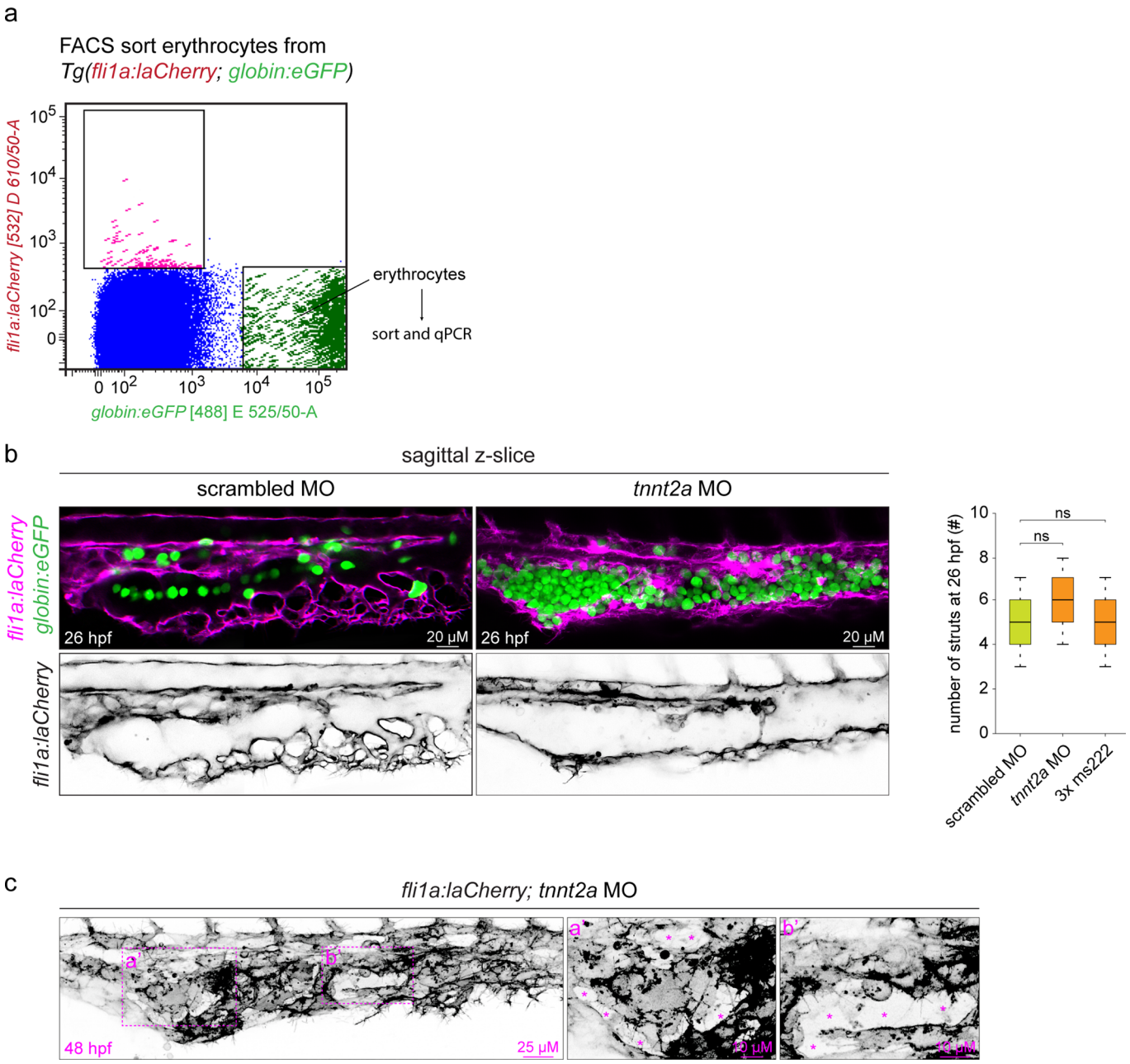

Extended Data Fig. 4 | Inhibition of blood flow prevents struts from pruning. a, Gating strategy used to FACS sort ECs from dissected CV regions followed by qPCR (**b**) The onset of blood flow was inhibited by either injecting of a *cardiac troponin T2a* (*tnnt2a*) MO or through administration of 3x concentrated ms-222 (tricaine methanesulfonate). Erythrocytes are marked by GFP (*globin*) and all ECs by laCherry (magenta). Data are presented as the median values with the first and third quartiles; the whiskers represent the minimum and maximum. One-way analysis of variance (ANOVA) with Dunn's post-hoc test. ns = not significant (n = 25 embryos per time points per experiment of three independent experiments). Images are representative of 5 embryos analysed by confocal microscopy per condition per experiment. **c**, 48 hpf embryo injected with *tnnt2a* MO. Asterisks indicate an incomplete formation of the CV wall. Images are representative of 10 embryos analysed from two independent experiments. Scale bars are defined in the figure.

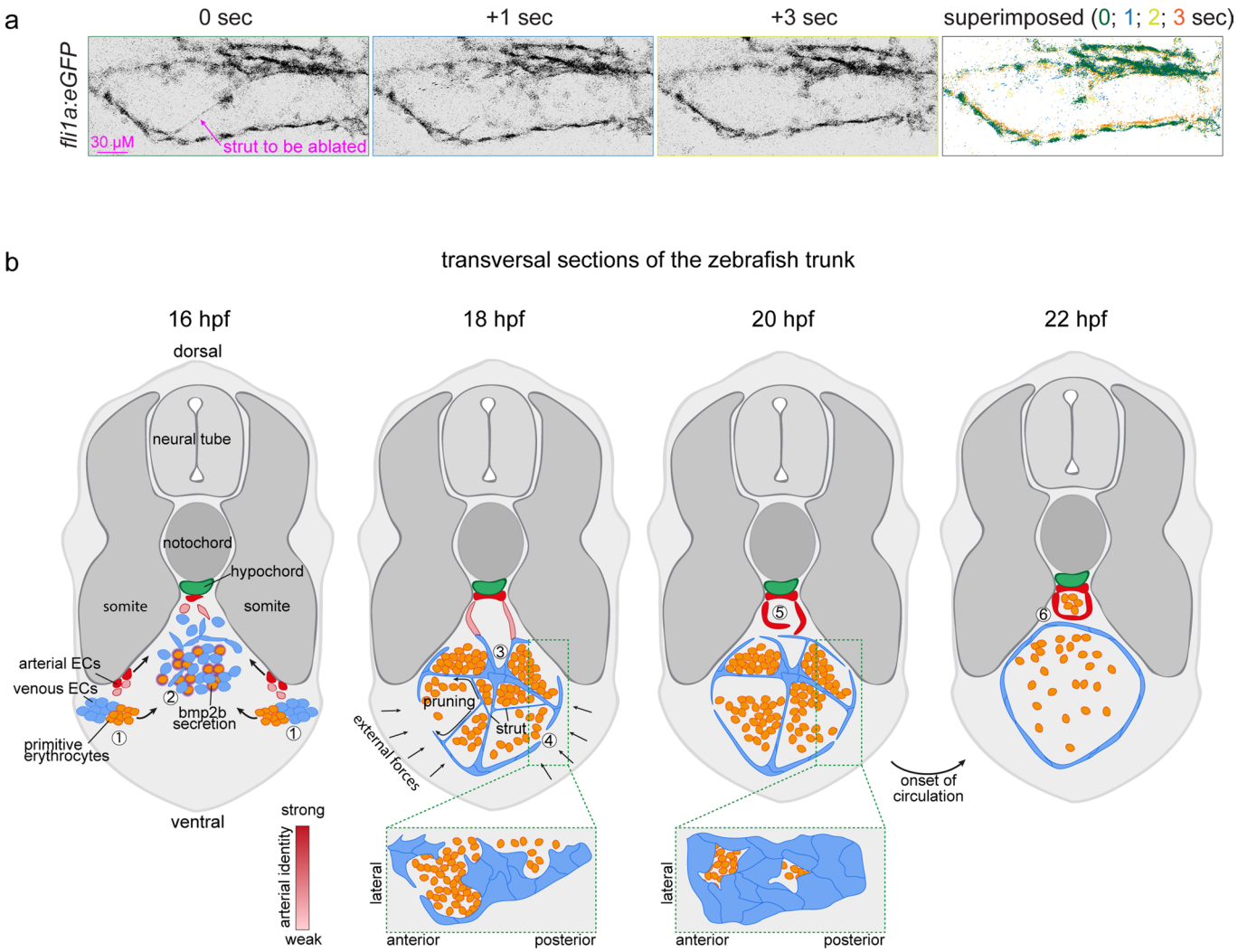

Extended Data Fig. 5 | Endothelial strut model. a, Laser ablation of a single strut resulted in a slight deformation of the CV, shown by the superimposed image of all timepoints. Stills are representative of 18 embryos analysed from three independent experiments. Scale bar is defined in the figure (**b**) Schematic. **1**) Venous (blue) and arterial (red) EC precursors originate from distinct locations within the lateral plate mesoderm, with the primitive erythrocytes (precursors) positioned medially adjacent to the venous ECs. **2**) ECs and erythrocytes migrate towards the midline of the embryo. Arterial ECs migrate along and directly contact the ventral face of the somites, thereby they receive inductive cues that strengthens the arterial fate (shades of red). **3**) At the midline, venous and arterial ECs coalesce into a network of struts and form a common precursor vessel. This process is bmp2b dependent, which is secreted by, among others, the erythrocytes. Strut formation encloses erythrocytes into compartments. **4**) The vessel wall consists initially only out of a few patches of ECs and upon pruning of struts, ECs from struts migrate into and are incorporated in the vessel wall. **5**) Arterial ECs participating in strut formation have a weak arterial identity, which progressively increases (shades of red) and results in the expression of the Notch target *efnb2b*, which drives the unmixing of arterial and venous ECs. Segregation of these arterial and venous ECs results in the formation of the DA and CV **6**) Onset of circulation flushes the *bmp2b* expressing erythrocytes from the CV, which is an important step for complete pruning of all struts. The lumen of the CV is now maintained by blood pressure rather than through the support of struts.

nature research

Corresponding author(s): David Traver and Bart Weijts

Last updated by author(s): February 8, 2021

Reporting Summary

Nature Research wishes to improve the reproducibility of the work that we publish. This form provides structure for consistency and transparency in reporting. For further information on Nature Research policies, see our Editorial Policies and the Editorial Policy Checklist.

Statistics

For all statistical analyses, confirm that the following items are present in the figure legend, table legend, main text, or Methods section.

n/a	Confirmed	
☐	☒	The exact sample size (*n*) for each experimental group/condition, given as a discrete number and unit of measurement
☐	☒	A statement on whether measurements were taken from distinct samples or whether the same sample was measured repeatedly
☐	☒	The statistical test(s) used AND whether they are one- or two-sided *Only common tests should be described solely by name; describe more complex techniques in the Methods section.*
☒	☐	A description of all covariates tested
☐	☒	A description of any assumptions or corrections, such as tests of normality and adjustment for multiple comparisons
☐	☒	A full description of the statistical parameters including central tendency (e.g. means) or other basic estimates (e.g. regression coefficient) AND variation (e.g. standard deviation) or associated estimates of uncertainty (e.g. confidence intervals)
☐	☒	For null hypothesis testing, the test statistic (e.g. *F*, *t*, *r*) with confidence intervals, effect sizes, degrees of freedom and *P* value noted *Give P values as exact values whenever suitable.*
☒	☐	For Bayesian analysis, information on the choice of priors and Markov chain Monte Carlo settings
☒	☐	For hierarchical and complex designs, identification of the appropriate level for tests and full reporting of outcomes
☒	☐	Estimates of effect sizes (e.g. Cohen's *d*, Pearson's *r*), indicating how they were calculated

Our web collection on statistics for biologists contains articles on many of the points above.

Software and code

Policy information about availability of computer code

Data collection	Zeiss Zen blue (version 3.0) Leica LAS X (version 3.4.2.18368)
Data analysis	Zeiss blue (version 3.0) Leica LAS X (version 3.4.2.18368) FIJI (version 1.52P) FIJI plugin MultiStackReg (to correct for drift version 1.45) Imaris (version 9.1) Imaris Sticher (version 9.1) R Statistical Package Version 3.4.0, R Core Team Adobe Illustrator, Photoshop, After Affects and Premiere (version CS5)

For manuscripts utilizing custom algorithms or software that are central to the research but not yet described in published literature, software must be made available to editors and reviewers. We strongly encourage code deposition in a community repository (e.g. GitHub). See the Nature Research guidelines for submitting code & software for further information.

Data

Policy information about availability of data

All manuscripts must include a data availability statement. This statement should provide the following information, where applicable:

- Accession codes, unique identifiers, or web links for publicly available datasets
- A list of figures that have associated raw data
- A description of any restrictions on data availability

All data supporting the findings of this study are available from the corresponding author on reasonable request.

Field-specific reporting

Please select the one below that is the best fit for your research. If you are not sure, read the appropriate sections before making your selection.

☒ Life sciences ☐ Behavioural & social sciences ☐ Ecological, evolutionary & environmental sciences

For a reference copy of the document with all sections, see nature.com/documents/nr-reporting-summary-flat.pdf

Life sciences study design

All studies must disclose on these points even when the disclosure is negative.

Sample size	Sample size (approximately n=20) were chosen based to garnish sufficient confidence between groups (Mead's Resource Equation). Animals were randomly picked from the entire clutch.
Data exclusions	No data was excluded at the post experimental stage. At the pre-experimental stage, a clutch was excluded if more than 10% of the embryos displayed obvious developmental defects.
Replication	All experiments were repeated at least two times (different day and breeding pair). All imaging data were successfully repeated by using different reporter lines (e.g. fli1a:eGFP, fli1a:mCherryCAAX, fli1a:lifeactCherry, KDR:eGFP). Except if the was no alternative transgenic line available: photoconversion (flk1:DENDRA, Fig. 1d and e), Notch reporter (TP1:eGFP, Fig. 2d), BMP reporter (BRE:eGFP, Fig. 3e)
Randomization	For each in vivo experiments, animals from the same clutch were divided into different treatment group without any bias (randomly distributed)
Blinding	Blinding was not performed as treated animals (e.g. chemically with BMP inhibitor or heat shock with noggin) can be easily distinguished from their control clutch mates due to their strong phenotype

Reporting for specific materials, systems and methods

We require information from authors about some types of materials, experimental systems and methods used in many studies. Here, indicate whether each material, system or method listed is relevant to your study. If you are not sure if a list item applies to your research, read the appropriate section before selecting a response.

Materials & experimental systems

n/a	Involved in the study
☒	☐ Antibodies
☒	☐ Eukaryotic cell lines
☒	☐ Palaeontology and archaeology
☐	☒ Animals and other organisms
☒	☐ Human research participants
☒	☐ Clinical data
☒	☐ Dual use research of concern

Methods

n/a	Involved in the study
☒	☐ ChIP-seq
☐	☒ Flow cytometry
☒	☐ MRI-based neuroimaging

Animals and other organisms

Policy information about studies involving animals; ARRIVE guidelines recommended for reporting animal research

Laboratory animals	Zebrafish (Danio rerio) were maintained and propagated according to the guidelines of the UCSD Institutional Animal Care and Use Committee (IACUC) and Hubrecht Institute ethical review board. All animal experiments were approved by the Animal Experimentation Committee (DEC) of the Royal Netherlands Academy of Arts and Sciences. Embryos and adult fish were raised in a circulating aquarium system (Aquaneering) at 28°C. The following zebrafish lines have been previously described: Tg(fli1a:lifeactCherry)ncv7Tg (ref 18) referred to as fli1a:laCherry; Tg(fli1a:eGFP)y1 (ref 30); Tg(hbbe1.1:EGFP)zf446 (ref 37) referred to as Tg(globin:eGFP); Tg(flk:DENDRA2) (ref 38); Tg(dll4:Gal4FF)hu10049Tg (ref 12); Tg(UAS:lifeactGFP)mu271 (ref 35) referred to as

	UAS:laGFP; Tg(EPV.Tp1-Mmu.Hbb:GFP-utrn) (ref 13) referred to as Tg(Tp1:GFP), Tg(hsp70:bmp2b) fr13 (ref 22), Tg(kdrl:nlsGFP)ubs1 (ref 6). Details on the strains and ages are noted for each experiment. Gender was not selected in any of the studies conducted.
Wild animals	This study did not involve wild animals.
Field-collected samples	This study did not involve samples collected from the field.
Ethics oversight	Zebrafish (Danio rerio) were maintained and propagated according to the guidelines of the UCSD Institutional Animal Care and Use Committee (IACUC) and Hubrecht Institute ethical review board. All animal experiments were approved by the Animal Experimentation Committee (DEC) of the Royal Netherlands Academy of Arts and Sciences.

Note that full information on the approval of the study protocol must also be provided in the manuscript.

Flow Cytometry

Plots

Confirm that:

☒ The axis labels state the marker and fluorochrome used (e.g. CD4-FITC).

☒ The axis scales are clearly visible. Include numbers along axes only for bottom left plot of group (a 'group' is an analysis of identical markers).

☒ All plots are contour plots with outliers or pseudocolor plots.

☒ A numerical value for number of cells or percentage (with statistics) is provided.

Methodology

Sample preparation	Embryos were collected and anesthetized in E3 medium containing 0.01% tricaine the CV region or trunk region was dissected and placed in ice-cold PBS. After centrifugation the pellet was washed with ice-cold PBS and resuspended TrypLE (ThermoFisher, 12563011) for 45min at 32 °C with vigorous shaking. Cells were then washed with FACS buffer (PBS + 2% FBS + 2mM EDTA), dissolved in FACS buffer + DAPI (ThermoFisher, 0.5ug/ml final concentration) and subsequently filtered through 40-µm nylon mesh. Cells were sorted on a FACS Aria II (BD Biosciences) and collected in FACS buffer for gene expression analysis.
Instrument	FACS Aria II (BD Biosciences)
Software	BD FACSDiva (version 8.0)
Cell population abundance	A minimum of 10.000 and maximum of 15.000 cells were sorted for mRNA extraction followed by quantitative PCR
Gating strategy	FSC and SSC were cut of 50K, live cells were DAPI negative (< 5x10^2). Gating strategy for erythrocytes (GFP) and endothelial cells (mCHerry) are shown in Extended Data Fig. 3b and 4a

☒ Tick this box to confirm that a figure exemplifying the gating strategy is provided in the Supplementary Information.